Spatial Analysis of Ensemble Learning Models for Agricultural Drought Early Warning

Sudianto Sudianto[1,*], Khoirun Ni'amah[2], Atika Ratna Dewi[3], Afan Ramadhan[4], Jeti Aprilia[5], Arsita Wiwit Tiyaswening[6], Syalaisha Nisrina Anataya[7]

[1]*Informatics Engineering Study Program, Telkom University, Purwokerto Campus, Indonesia*

[3,4,5,6,7]*Data Science Study Program, Telkom University, Purwokerto Campus, Indonesia*

[2]*Telecommunication Engineering Study Program, Telkom University, Purwokerto Campus, Indonesia*

(Received: August 10, 2025; Revised: October 10, 2025; Accepted: December 28, 2025; Available online: January 31, 2026)

Abstract

Drought poses a serious threat to rice production and local food security, triggered by climate anomalies such as El Niño. This study aims to evaluate and compare the performance of Ensemble Learning Models in classifying drought levels and analyze its correlation with periods of climate anomalies. This study uses Landsat 9 image data in the simulation period from June 2024 to July 2025, which is processed with HSV-based pan-sharpening and spectral index extraction (NDVI, NDWI, NDDI, EVI, LST). The modeling process applied undersampling to address class imbalance and hyperparameter tuning optimization using Optuna. The models compared included Random Forest, LightGBM, AdaBoost, XGBoost, and Gradient Boosting. The results showed that Gradient Boosting excelled with a train accuracy of 96,85% in original dataset with split dataset 70:30, whereas rise to 98.98% after tuning. Spatial validation was conducted in other rice field plots, however its steadfastly on research area with same treatment. The classification map shows the dominance of the moderate category, which temporally coincides with the period of rainfall decline associated with El Niño, although a direct causal relationship requires further investigation. These findings confirm that remote sensing combined with machine learning is effective for drought monitoring, with the caveat that the application of undersampling and limited spatial validation that is, confined solely to the research area; needs to be considered in the interpretation of results.

Keywords: El Niño, Ensemble Learning, Landsat 9, Drought Prediction, Remote Sensing

1. Introduction

Drought is one of the most detrimental hydrometeorological disasters, having a significant impact on the agricultural sector in Indonesia, particularly on rice fields. The increasingly intense phenomenon of global climate change, exacerbated by climate anomalies such as El Niño 2024, has increased the frequency and intensity of extreme weather events that disrupt the balance between rainfall and crop water requirements [1]. El Niño, through the rise of sea surface temperatures in the central Pacific region, triggers a significant decrease in rainfall, directly affecting rice productivity and national food security [2]. This phenomenon has led to losses and potential crop failures in almost all regions of Indonesia, thereby necessitating solutions to predict the classification level of affected crops. Such predictions can provide information to farmers about areas requiring intervention and further actions to prevent or mitigate losses.

Remote sensing technology has become one of the most effective approaches for drought monitoring due to its ability to provide extensive, continuous, and efficient spatial-temporal data [3]. Various vegetation indices, such as NDVI, NDWI, and NDDI, have proven reliable in detecting vegetation stress levels and soil moisture [4]. In addition, the inclusion of EVI and LST indices further refines information and parameters related to plant health and soil temperature, which are essential for credible modeling details. The accuracy of drought detection has been further enhanced through the integration of Machine Learning methods, particularly Ensemble Learning techniques such as Random Forest, LightGBM, XGBoost, AdaBoost, and Gradient Boosting, which exhibit high robustness against data noise [5]. The selection of the five models for further evaluation was based on an initial assessment of ten different

***Corresponding author: Sudianto (sudianto@telkomuniversity.ac.id)**
DOI: https://doi.org/10.47738/jads.v7i1.1108

ISSN 2723-6471

models. Among these, the five selected models demonstrated the most superior and consistent performance, making them suitable for continued analysis. Nevertheless, research gaps still exist, primarily because most studies focus on macro scales (e.g., island or provincial levels) and have yet to conduct extensive validation at the micro scale (village level), which represents the smallest agricultural management unit [6]. Furthermore, comprehensive comparisons of ensemble model performance in the context of agricultural drought in Indonesia remain limited [7], [8].

This study aims to fill the existing research gap through a comparative analysis of paddy field drought levels at a local scale. The case study was conducted in Dawuhan Village, Banyumas Regency, Central Java, an area of rainfed rice fields with high vulnerability to rainfall reduction during the El Niño period in Indonesia. The data used were derived from Landsat 9 satellite imagery with two main objectives: (1) to evaluate and compare the performance of five ensemble learning models Random Forest, LightGBM, AdaBoost, XGBoost, and Gradient Boosting in classifying drought levels and (2) to identify drought conditions in rice fields and their relationship with the El Niño period. The results of this research are expected to provide recommendations for the best model to support the development of a post-drought classification system, thereby enabling more precise and applicable agricultural practices at the regional level to mitigate losses promptly and minimize the reduction of productive farming time. Furthermore, the findings are expected to offer practical contributions to local food security amid the increasing threat of climate variability [9].

2. Related Work

Based on previous studies conducted by other authors, many have utilized satellite-based imagery data and demonstrated success with significant advancements, resulting in effective drought analyses as well as other applications [10], [11], [12]. These findings indicate that satellite imagery data still hold great potential for further exploration, particularly in the indices derived from band calculations provided by each satellite type. The integration of NDVI, NDWI, NDDI, EVI, and LST represents a complex combination that is rarely employed by researchers as indicators for precise drought prediction [12], [13]. This study merged the indices mentioned before with ensemble models that a technique of machine learning who is made by several predictions from multiple base learners to improve accuracy, stability, and generalization performance compared to a single model [14]. Indeed, the incorporation of data augmentation technique has made the model dominant approach across numerous application domaint, owing to its ability to reduce errors and effectively manage data variability [15]. Several studies have begun applying machine learning algorithms to generate predictions; however, research comparing variations of ensemble learning models remains scarce [14]. One such study found that a combination of ensemble models, apart from the five models compared in our research, performed best, including CatBoost Regressor (CBR), Extra Trees Regressor (ETR), Extreme Gradient Boosting (XGB), Light Gradient Boosting Machine (LGBM), and Random Forest (RF). Many studies conclude once they determine that the Random Forest algorithm is highly effective for processing satellite-based imagery data. In this study, we compare the Random Forest algorithm with Light Gradient Boosting Machine, AdaBoost, Extreme Gradient Boosting, and Gradient Boosting, all of which are based on Ensemble Learning [15]. Existing research also tends to train data and stop after obtaining the best accuracy value. This study includes a hyperparameter tuning process to enhance each model's performance and produce accuracy values that provide greater utility for prediction outputs [16]. The use of Optuna as a hyperparameter optimization framework automates the search for the best parameters, eliminating the need for manual tuning that risks misinterpretation. In addition, our study employs an undersampling method to trim data so that class proportion alignment does not leave a majority class with unnecessary interpretive dominance. This method is more effective than oversampling, which increases data through synthetic generation and, when applied to models, can heighten the probability of algorithmic bias [17]. The Ensemble Learning models we compare have been optimized through hyperparameter tuning using Optuna to determine the best parameters for training the dataset before generating predictions. Thus, our research fills a gap in agricultural drought classification prediction, particularly for rice varieties, through tuning and ensemble learning models.

ISSN 2723-6471

3. The Proposed Method

Figure 1 illustrates the research workflow, starting from ROI cropping, labeling, and indices extraction to obtain vegetation index values. The process continues with modeling using both the original and undersampled data, followed by hyperparameter tuning using Optuna for model optimization. The undersampling method was chosen because the dataset for training was sufficient and produced a good evaluation, but there was class imbalance in each index which could potentially result in biased results, while oversampling was not chosen because it would increase the data but synthetic which would affect the inaccuracy of the prediction. Evaluation is conducted through performance metrics and learning curves to identify the two best-performing models with the highest accuracy.

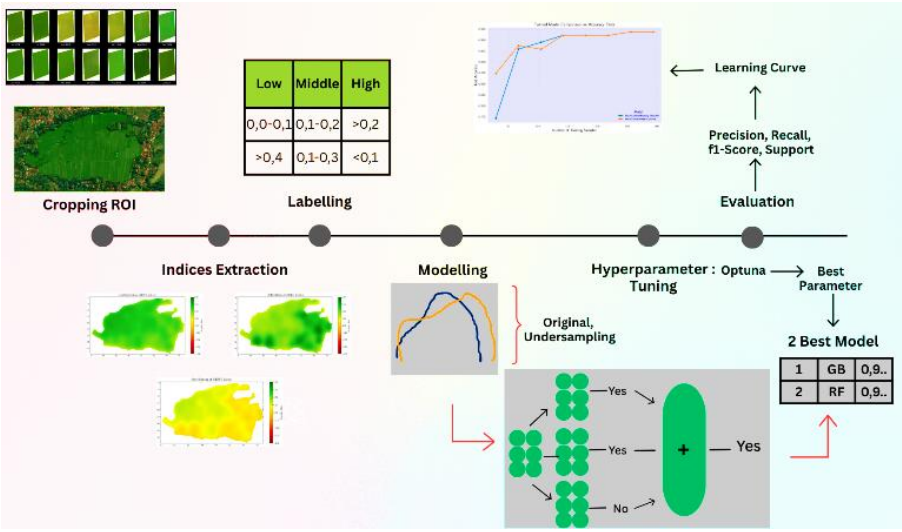

Figure 1. Flow diagram in building classification model to predict risk drought on rice plants

Workflow to process dataset until result in this research has a step in above, that is start with cropping ROI that spesifically on part of the rice fields in research area and then pick best image that is clearly from the clouds, smooky, or broken image. Clean image helps data extraction and enrich data variation; this is needed in model training. After that, we can extract data from images which partition in indices; example NDVI, NDWI, NDDI, EVI, and LST thus discovered variables to uphold the result. The data mentioned must labeled by a parameter that suitable for specific indices according to formula of every indices. Then we must enter the dataset in model with 2 schema which is original and undersampling, subsequently enter the ensemble learning base models in training that resulting best model; this maximized with hyperparameter tuning by optuna that search best parameter, therefore best result can be achieve.

3.1. Research Data

This study focuses on paddy field areas in Dawuhan Village, Banyumas Regency, Central Java. The location was selected as the ROI (Region of Interest, figure 2) because it represents an active agricultural area that has factually cultivated various rice varieties over the past five years, aligning with the research objectives. This condition makes the area representative for examining the dynamics of vegetation indices and land surface temperature in paddy fields relevant to the study's focus. The El Niño climate anomaly that occurred during the 2023-2025 period is strongly suspected to have triggered a significant decrease in rainfall within the ROI, leading to an increased risk of drought and potential crop failure.

Figure 2. Research Area

 ISSN 2723-6471

To monitor these conditions, this study utilizes remote sensing data from Landsat 9 OLI/TIRS Collection 2 Top-of-Atmosphere (TOA) satellite imagery. The analysis was conducted on images from Path 120–121 and Row 065, covering the period from June 2024 to July 2025, corresponding to the drought observation timeframe. The satellite imagery used has a spatial resolution of 30 meters. The spectral bands extracted for analysis include B2 (Blue), B3 (Green), B4 (Red), B5 (Near-Infrared/NIR), B6 (Shortwave Infrared 1/SWIR1), B8 (Panchromatic), and B10 (Thermal Infrared).

3.2. Data Preprocessing

To enhance the spatial resolution of the multispectral imagery, a pan-sharpening technique based on Hue-Saturation-Value (HSV) fusion was applied. This method integrates the panchromatic band (B8), which has a 15-meter resolution (figure 3), with the RGB composite image (B4, B3, B2) at a 30-meter resolution. The fusion process is performed by transforming the RGB color space into HSV, replacing the Value (V) component with data from the panchromatic band, and then converting it back to the RGB color space, as formulated in Equation (1a).

$$R_{out} = \left(\frac{R_{in}}{R_{in} + G_{in} + B_{in}}\right) \times P_{in} \tag{1a}$$

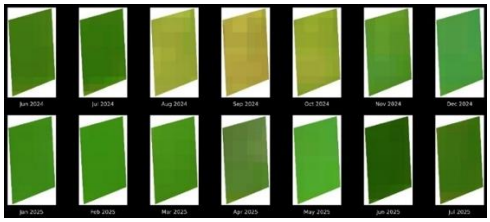

Figure 3. Pansharpened

The result of this process is a multispectral image with an effectively enhanced spatial resolution of 15 meters, allowing for more detailed vegetation analysis. The HSV method was chosen for its ability to effectively preserve spectral integrity, which is crucial for minimizing potential distortions in the calculation of vegetation indices such as NDVI and NDWI used in subsequent analyses.

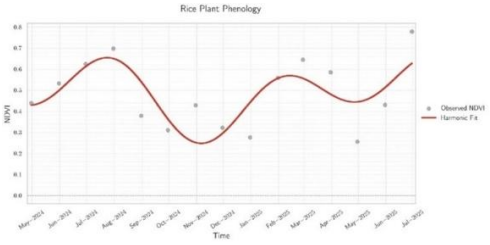

Figure 4. The phenology of rice plants in ROI

This phenological analysis utilizes a harmonic model to model the rice growth cycle based on NDVI time-series data. This model describes the growth pattern of plants as a periodic function consisting of constant and harmonic components, as formulated in Equation (1a).

$$Y_t = \beta_0 + \beta_1 t + \sum_{k=1}^{H} (\alpha_k \cos(2\pi k t) + \gamma_k \sin(2\pi k t)) + \epsilon_t \tag{1b}$$

Phenological analysis was conducted using a harmonic model on the NDVI time-series data May 2024 - July 2025 to establish a baseline of normal rice growth patterns. The modeling results shown in figure 4 confirm the presence of a double-cropping system, with phenological peaks detected in July-August 2024 and February-March 2025, consistent with the local planting calendar. This phenological baseline serves as an important reference to distinguish NDVI value declines caused by drought stress from natural decreases due to the maturation and harvesting phases.

Based on this reference, a feature extraction process was carried out using remote sensing imagery to obtain several spectral indices representing vegetation condition, moisture, and land surface temperature in paddy fields. The indices

used include NDVI, NDWI, NDDI, EVI, and LST, each serving a specific function in describing vegetation greenness, soil moisture content, and drought intensity [18], [19]. The formulas for each index are presented as follows.

$$NDVI = \frac{NIR - RED}{NIR + RED} \quad (2)$$

$$NDWI = \frac{NIR - SWIR}{NIR + SWIR} \quad (3)$$

$$NDDI = \frac{NDVI - NDWI}{NDVI + NDWI} \quad (4)$$

$$EVI = G \times \frac{(NIR - RED)}{(NIR + C_1 \times RED - C_2 \times BLUE + L)} \quad (5)$$

$$LST = \frac{BT}{1 + \left(\frac{\lambda \times BT}{\rho}\right) ln(\varepsilon)} \quad (6)$$

Threshold determination was carried out to separate drought severity levels so that the classification output can be utilized in an early warning system. The classification scale consists of three categories: Low, Middle, and High. The Low category indicates non-drought conditions, characterized by high NDVI and NDWI values, high EVI, and low NDDI and LST values. The Middle category represents moderate conditions, with indicator values in the mid-range, signifying the initial stage of moisture reduction. The High category indicates severe drought conditions, characterized by low NDVI, NDWI, and EVI values, along with high NDDI and LST values, which reflect a significant decline in vegetation. The threshold parameter is based on a number of specific studies by calculating the value of each index [20], [21], [22], [23], [24], [25], in addition the value is taken from observations of each value generated from the image, such as if the NDVI score is 0.6 then it is classified as healthy and not dry accompanied by an image clear of clouds and the rice fields look green and clear.

Table 1. Threshold

Index	Low	Middle	High
NDVI	> 0.6	0.4-0.6	< 0.4
NDDI	< 0.25	0.25-0.38	> 0.38
NDWI	>0.3	0.2-0.3	<0.2
EVI	> 0.3	0.2-0.3	<0.2
LST	< 25	25-28	> 28

3.3. Trends Index

Figure 5 presents the monthly median trends of the indices used to monitor vegetation and drought conditions, namely NDWI, NDDI, and NDVI. The horizontal axis represents the time range from June 2024 to July 2025, while the vertical axis shows the monthly median index values. Correlation analysis among the three indices reveals a significant relationship an increase in NDDI values (indicating drought conditions) is negatively correlated with a decrease in NDWI and NDVI values.

Conversely, periods with high moisture levels (indicated by a decrease in NDDI) are accompanied by increases in NDWI and NDVI values. The interpretation of this pattern indicates that the most severe drought period was observed within the highlighted range (September–December 2024), with the drought peak occurring in October–November 2024. During this drought period, when rainfall dropped below 100 mm, indications of drought-related environmental impacts began to emerge, as reflected in the changes in NDVI, NDWI, and NDDI values. Such conditions reflect the heightened stress on agricultural land during drought periods [19].

 ISSN 2723-6471

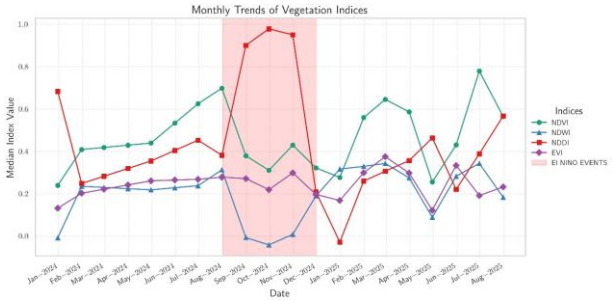

Figure 5. Monthly Trends of Vegetation Index

This situation has serious implications for potential yield reduction, as water shortages during the grain-filling stage can lead to empty or unfilled rice grains. These findings reinforce reports from BMKG and FAO, while also providing spatial and temporal evidence of El Niño's impact on the agricultural sector.

3.4. Model Comparison

Model comparison is an evaluation process conducted to assess and compare the performance of various machine learning algorithms in order to identify the model with the best performance for a given dataset. This process involves testing different parameter variations, training–testing data ratios, and the application of data balancing methods. Through this approach, researchers can evaluate the effectiveness of each algorithm based on evaluation metrics such as accuracy, precision, recall, F1-score, and computational time. In this study, the comparison process focuses on ensemble learning models, which are known for their high generalization capability by combining multiple weak learners to form a strong learner. The ensemble models used include Random Forest, LightGBM, AdaBoost, XGBoost, and Gradient Boosting, each possessing distinct characteristics and learning mechanisms to enhance predictive performance.

3.4.1. Random Forest Algorithm

Random Forest was chosen for its ability to handle multidimensional data from various spectral indices (NDVI, NDWI, NDDI, EVI, LST) and its resistance to overfitting. In the context of drought detection, this model effectively identifies non-linear patterns in the relationship between vegetation indices and the water stress level of rice plants. In addition, the feature importance of Random Forest also helps identify which indices are most influential in drought classification. [26], [27] The final model prediction is determined through a voting process for classification tasks or through averaging for regression tasks, as stated in Equation (7).

$$\hat{y} = \frac{1}{T}\sum_{t=1}^{T} h_t(x) \tag{7}$$

T represents the total number of trees and $h_t(x)$ denotes the prediction result from the-t tree.

3.4.2. Light Gradient Boosting Machine (LightGBM)

LightGBM is optimized for computational efficiency on time-series data such as the Landsat time series used. Its native handling of missing values is well suited for satellite data, which is often contaminated by clouds [21]. In addition, its native ability to handle missing values is well suited to satellite data, which is often contaminated by clouds. In the context of drought detection, the efficient leaf-wise construction of this model enables the detection of subtle changes in vegetation conditions, which can indicate early-stage drought. This model constructs a tree (decision tree) in a leaf-wise manner to minimize the loss function, as formulated in Equation (8)

$$L = \sum_{i=0}^{n} l\left(y_i . \hat{y}_i + f_t(x_i)\right) + \Omega(f_i) \tag{8}$$

$l()$ denotes the loss function. f_t represents the newly added the-t tree, and. and $\Omega(f_t)$ is the regularization component.

3.4.3. Adaboost

AdaBoost is applied to improve classification accuracy at the boundary between drought categories [29]. This objective is achieved through the adaptive boosting mechanism in AdaBoost, which effectively focuses learning on samples that are difficult to classify [30] as formulated in Equation (9). In the context of drought, this approach helps to sharply distinguish between moderate and severe drought conditions

$$H(x) = sign\left(\sum_{t=1}^{T} \alpha_t h_t(x)\right) \tag{9}$$

3.4.4. Extreme Gradient Boosting (XG Boost)

The potential for multicollinearity that often occurs between vegetation indices is handled using XGBoost, which implements the L1/L2 regularization mechanism [31]. This regularization mechanism has been proven effective in maintaining model generalization, even in datasets with high feature correlation [32].

$$Objective^{(p)} = \sum_{k=1}^{n} l\left(\bar{y}_i . y_i\right) + \sum_{k=1}^{p} \Omega\left(f_i\right) \tag{10}$$

$\Omega(f)$ is the regularization function that controls model complexity. XGBoost is well known for its efficiency, capability to handle large-scale data, and high performance across various types of datasets.

3.4.5. Gradient Boost

Gradient Boosting (GB) was implemented to capture the temporal progression of drought stress through a sequential learning approach. This approach was realized through a stage-wise construction mechanism in Gradient Boosting, which is highly effective for modeling gradual processes such as the deterioration (decline) of vegetation conditions. This mechanism allows the model to iteratively correct errors in identifying stages of drought.

$$F_m(x) = F_{m-1}(x) + v . H_m(x) \tag{11}$$

3.5. Model Classification

This analysis aims to evaluate the performance of five ensemble classification models: XGB Classifier, Random Forest, LGBM, Gradient Boosting, and AdaBoost. The performance of each model is assessed based on the metrics of Accuracy, Recall, F1-score, Precision, and computational time, with detailed results presented in table 2. Given the significant class imbalance in the dataset, resampling was deemed necessary. Undersampling using the Cluster Centroids technique was selected over oversampling primarily to mitigate the risk of introducing synthetic noise and overfitting, which can be prevalent in oversampling methods like SMOTE, especially when the minority class is small. This approach also reduces computational cost, aligning with the objective of evaluating model efficiency. Model testing was conducted under two data scenarios the original dataset and the dataset processed using the Cluster Centroids undersampling technique. Validation was performed using two different data split ratios, namely 70:30 and 80:20.

Table 2. Comparison of Ensemble Learning

Model	Split	Dataset	Accuracy	Precision Score	Recall Score	F1 Score	Time Passed (s)
Random Forest	80:20	Original	0.9529	0.954	0.9529	0.9528	0.1089
	70:30	Original	0.9685	0.969	0.9685	0.9684	0.1259
	80:20	Undersampling	0.9412	0.9419	0.9412	0.9409	0.1293
	70:30	Undersampling	0.9528	0.9534	0.9528	0.9527	0.1256
XGBoost	80:20	Original	0.9528	0.9534	0.9528	0.9527	0.6677
	70:30	Original	0.9412	0.9440	0.9412	0.9414	0.3744

LightGBM	80:20	Undersampling	0.9412	0.9440	0.9412	0.9414	0.3487
	70:30	Undersampling	0.9370	0.9397	0.9370	0.9371	0.3400
	80:20	Original	0.9529	0.9540	0.9529	0.9528	0.3279
	70:30	Original	0.9685	0.9690	0.9685	0.9684	0.3039
	80:20	Undersampling	0.9529	0.9540	0.9529	0.9528	0.2144
	70:30	Undersampling	0.9606	0.9621	0.9606	0.9607	0.2038
AdaBoost	80:20	Original	0.9176	0.9182	0.9176	0.9161	0.4225
	70:30	Original	0.9370	0.9375	0.9370	0.9363	0.4173
	80:20	Undersampling	0.9294	0.9391	0.9294	0.9288	0.3288
	70:30	Undersampling	0.9055	0.9242	0.9055	0.9048	0.3121
Gradient Boosting	80:20	Original	0.9529	0.9540	0.9529	0.9528	1.0254
	70:30	Original	0.9s685	0.9690	0.9685	0.9684	0.9675
	80:20	Undersampling	0.9529	0.9540	0.9529	0.9528	0.8308
	70:30	Undersampling	0.9606	0.9610	0.9606	0.9605	0.8880

4. Results and Discussion

4.1. Building a Recommendations Model using Ensemble Learning

In this study, several classification models were tested to develop a model capable of classifying drought levels in rice fields based on NDVI, NDWI, NDDI, EVI, and LST values. Based on the performance comparison of the five models, two top-performing models with equal accuracy values were identified, prompting the implementation of hyperparameter tuning to determine the model with the best accuracy.

Table 3 presents the final results of the hyperparameter tuning process conducted on the two best-performing models, namely Random Forest and Gradient Boosting. The objective of this optimization process was to identify the most effective combination of parameters to maximize drought classification accuracy. achieved an accuracy of approximately 99% lies in its fundamental learning mechanism. Its boosting method operates sequentially, where models are built stage by stage. This contrasts with Random Forest (a bagging method), which runs multiple models in parallel and independently. The sequential approach allows Gradient Boosting to continuously correct its own errors each new decision tree is designed to address the weaknesses of the previous one. In the context of drought classification, this means the model iteratively becomes more “intelligent” in recognizing complex patterns, particularly in borderline classification cases. As a result, this model can construct more accurate decision boundaries and demonstrate superior performance, as illustrated in figure 6.

Table 3. Best Hyperparameters after Tuning

Model	Accuracy	Parameter
Random Forest	0.976271	{'n_estimators': 120, 'max_depth': 15, 'min_samples_split': 2, 'min_samples_leaf': 1, 'max_features': 'sqrt'}
Gradient Boosting	0.989831	{'n_estimators': 198, 'learning_rate': 0.2663611389836013, 'max_depth': 7, 'min_samples_split': 12, 'min_samples_leaf': 7, 'subsample': 0.7553174659892969, 'max_features': 'sqrt'}

 ISSN 2723-6471

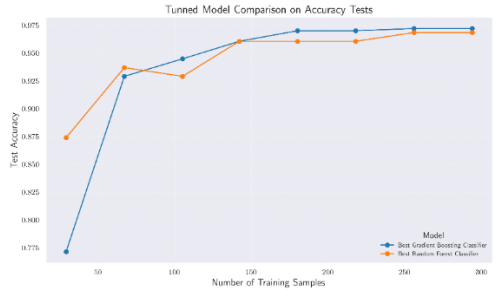

Figure 6. Learning Curve on Accuracy Test

Figure 6 shows that the accuracy of both models increases with the number of training samples. At smaller sample sizes, both models exhibit fluctuations in accuracy, but Random Forest and Gradient Boosting display a similar upward trend up to around 150 samples. Overall, Gradient Boosting achieves the highest accuracy of around 0.97, indicating superior performance in drought level classification.

4.2. Drought Levels Classification

The feature extraction results presented in the table and visualization display the NDVI, NDWI, NDDI, EVI, and LST indices obtained from remote sensing imagery, which were then used for classification. The classification was based on predetermined threshold values, as shown in table 4. The classification results are presented in the prediction column with three labels, label 0 indicates normal conditions or areas with high soil moisture, label 1 represents moderate drought, where vegetation begins to decline, and surface temperature increases, and label 2 indicates severe drought, characterized by low NDVI and NDWI values, as well as high NDDI and LST values.

Table 4. Feature Extraction

No	NDVI	NDWI	NDDI	EVI	LST	Pred
1	0.5266	0.1756	0.4998	0.4281	25.4893	0
2	0.6200	0.1969	0.5178	0.4550	25.4650	0
3	0.5805	0.1993	0.4886	0.4062	25.5891	1
4	0.4901	0.1178	0.6122	0.4039	25.5825	1
5	0.4901	0.1178	0.6122	0.4039	25.5825	1
…	...	…	…	…	…	…
766	0.4737	0.0305	0.8787	0.3867	25.8020	2
…	…	…	…	…	…	…
2060	0.6061	0.1744	0.5531	0.4277	25.6296	1
2061	0.5802	0.1507	0.5874	0.4103	25.6134	1
2062	0.5802	0.1507	0.5874	0.3809	25.6134	1
2063	0.6061	0.1744	0.5531	0.4441	25.6296	1
2064	0.5802	0.1507	0.5874	0.3637	25.6134	1

The distribution of these labels is shown in figure 7, providing an overview of the proportion of each drought condition class and helping evaluate data balance. This information is also essential to ensure that the training process is not dominated by a specific class.

ISSN 2723-6471

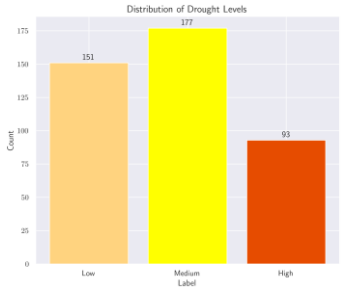

Figure 7. Distribution Drought Levels

4.3. Drought Severity Prediction Results

Figure 8 shows the spatial distribution of drought vulnerability levels classified into three categories: Low, Moderate, and Severe. This visualization represents the vulnerability conditions during the period from June 2024 to July 2025, which coincides with the 2024–2025 El Niño climate anomaly period based on BMKG reports.

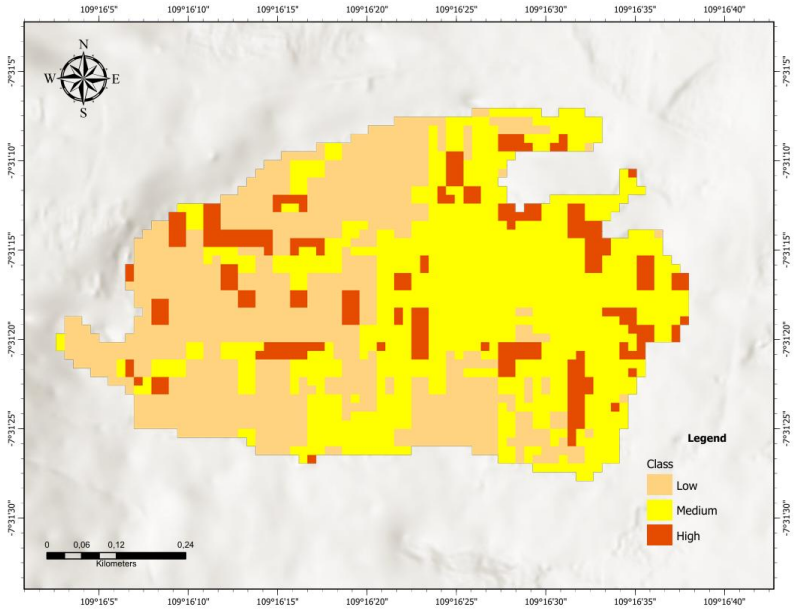

Figure 8. Prediction of drought levels on ROI

The dominance of the Moderate category across most areas indicates that the rice fields in the study region experienced significant drought stress but had not yet reached a critical stage. When contextualized with the timing of events, this pattern of vulnerability distribution aligns with the impacts of El Niño reported in previous studies, where Pacific sea surface temperature anomalies tend to suppress rainfall across Indonesia.

These findings reinforce the assumption that the El Niño period has the potential to increase the vulnerability of rice fields to drought, although a direct causal relationship requires further investigation through the integration of more comprehensive climate data.

4.4. Drought Risk Prediction Based on Ensemble Learning Model

The drought prediction system was developed as an interactive web application to facilitate accessible, real-time monitoring for end-users. By directly integrating Landsat remote sensing indices (NDVI, NDWI, NDDI, EVI, and LST), the system allows users to analyze biophysical land conditions without requiring programming skills or complex image processing expertise. This approach aligns with modern trends in geospatial decision-support systems, which prioritize ease of access and the automation of spatial data processing. Through the dashboard, as illustrated in figures 9 and figure 10, users can filter imagery based on temporal range and cloud cover to ensure optimal data quality. Once a representative image is selected and the Area of Interest (AOI) is delineated, the system automatically extracts

ISSN 2723-6471

vegetation and thermal indices to feed a pre-trained drought prediction model. The results are visualized as thematic maps and statistical distributions of drought severity (low, medium, high), enabling rapid and accurate spatial assessment.

This integrated workflow enhances both monitoring accuracy and operational efficiency by automating the entire pipeline from feature extraction to prediction within a single platform. Consequently, the system is highly applicable for agricultural monitoring, risk mitigation, and climate change adaptation strategies at both local and regional scales.

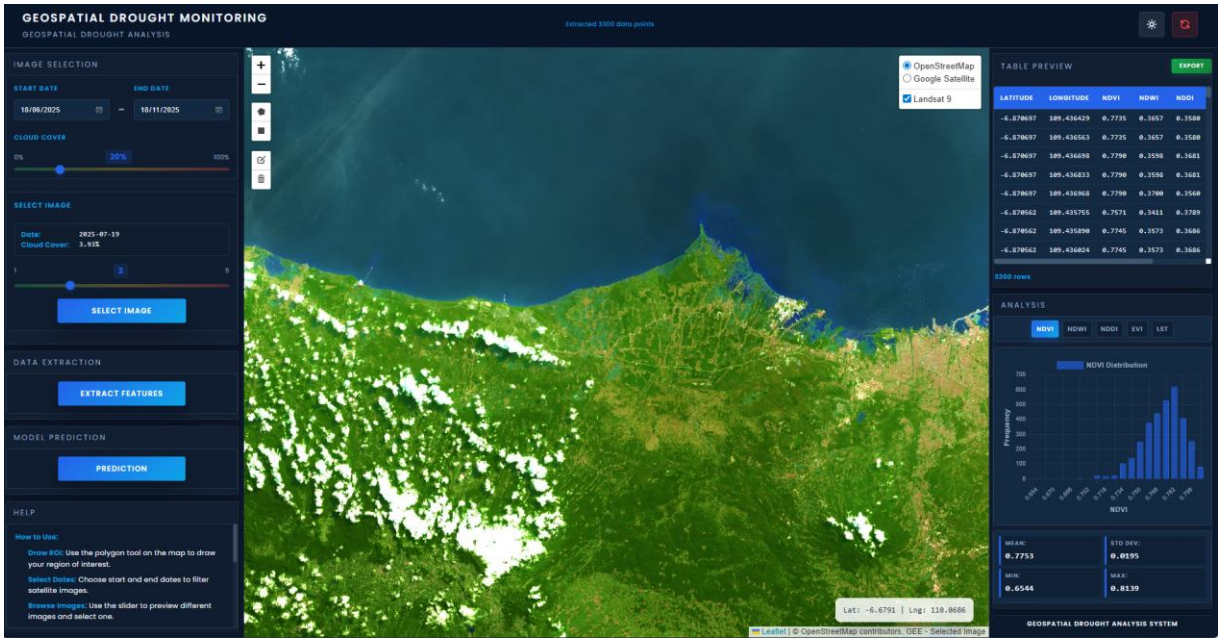

Figure 9. Dashboard Classification of Drought Levels

Figure 10. Drought Level Percentage Dashboard

5. Conclusion

This study successfully mapped and classified the level of drought vulnerability of rice fields in Dawuhan Village by utilizing Landsat 9 imagery and an ensemble learning approach. A comparison of five models (Random Forest, LightGBM, AdaBoost, XGBoost, and Gradient Boosting) showed that Gradient Boosting excelled with an accuracy of

98.98% after tuning. The classification results were dominated by the moderate category during the 2024 El Niño period, which is consistent with the pattern of rainfall decline associated with this phenomenon. This approach has proven to be effective for objective drought classification, as reflected by the high model accuracy achieved after tuning. The limitations of the study include the lack of consideration of socio-economic and irrigation factors, as well as validation limited to one region. Further research is recommended to expand the test area and integrate global climate data such as the Oceanic Nino Index (ONI).

6. Declarations

6.1. Author Contributions

Conceptualization: S.S., K.N., A.R.D., A.R., J.A., A.W.T., and S.N.A.; Methodology: S.S.; Software: S.S.; Validation: S.S., K.N., and A.R.D.; Formal Analysis: S.S., K.N., and A.R.D.; Investigation: S.S.; Resources: K.N.; Data Curation: K.N.; Writing Original Draft Preparation: S.S., K.N., and A.R.D.; Writing Review and Editing: K.N., S.S., and A.R.D.; Visualization: S.S. All authors have read and agreed to the published version of the manuscript.

6.2. Data Availability Statement

The data presented in this study are available on request from the corresponding author.

6.3. Funding

The authors received no financial support for the research, authorship, and/or publication of this article.

6.4. Institutional Review Board Statement

Not applicable.

6.5. Informed Consent Statement

Not applicable.

6.6. Declaration of Competing Interest

The authors declare that they have no known competing financial interests or personal relationships that could have appeared to influence the work reported in this paper.

References

[1] A. AghaKouchak , “Remote sensing of drought: Progress, challenges and opportunities,” *Rev. Geophys.*, vol. 53, no. 2, pp. 452–480, Jun. 2015, doi: 10.1002/2014RG000456.

[2] G. M. Gandhi, S. Parthiban, N. Thummalu, and A. Christy, “NDVI: Vegetation change detection using remote sensing and GIS—A case study of Vellore district,” *Procedia Comput. Sci.*, vol. 57, no. 1, pp. 1199–1210, Jul. 2015, doi: 10.1016/j.procs.2015.07.415.

[3] N. Sánchez, J. Martínez-Fernández, and A. González-Zamora, “A combined approach with SMOS and MODIS to monitor agricultural drought,” *Int. Arch. Photogramm. Remote Sens. Spatial Inf. Sci.*, vol. XLI-B8, pp. 393–398, 2016, doi: 10.5194/isprsarchives-XLI-B8-393-2016.

[4] Q. Qin , “Optical and thermal remote sensing for monitoring agricultural drought,” *Remote Sens.*, vol. 13, no. 24, pp. 1–25, Dec. 2021, doi: 10.3390/rs13245092.

[5] X. Zhang , “Remote sensing object detection meets deep learning: A meta-review of challenges and advances,” *arXiv preprint*, Sep. 2023. [Online]. Available: http://arxiv.org/abs/2309.06751

[6] L. F. Amalo, R. Hidayat, and S. Sulma, “Analysis of agricultural drought in East Java using vegetation health index,” *Agrivita*, vol. 40, no. 1, pp. 63–73, Feb. 2018, doi: 10.17503/agrivita.v40i1.1080.

[7] F. A. Prodhan , “Deep learning for monitoring agricultural drought in South Asia using remote sensing data,” *Remote Sens.*, vol. 13, no. 9, pp. 1–23, May 2021, doi: 10.3390/rs13091715.

[8] I. H. Houmma, L. El Mansouri, S. Gadal, M. Garba, R. Hadria, and H. Rachid, “Modelling agricultural drought: A review of latest advances in big data technologies,” *Int. J. Digit. Earth*, vol. 15, no. 1, pp. 1–22, Nov. 2022, doi: 10.1080/19475705.2022.2131471.

[9] M. Dimyati , "Spatiotemporal relation of satellite-based meteorological to agricultural drought in the downstream Citarum watershed, Indonesia," *Environ. Sustain. Indicators*, vol. 22, pp. 1–12, Jun. 2024, doi: 10.1016/j.indic.2024.100339.

[10] J. Khan, P. Wang, Y. Xie, L. Wang, and L. Li, "Mapping MODIS LST–NDVI imagery for drought monitoring in Punjab, Pakistan," *IEEE Access*, vol. 6, pp. 19898–19911, Mar. 2018, doi: 10.1109/ACCESS.2018.2821717.

[11] H. Luo, J. Bhardwaj, S. Choy, and Y. Kuleshov, "Applying machine learning for threshold selection in drought early warning system," *Climate*, vol. 10, no. 7, pp. 1–12, Jul. 2022, doi: 10.3390/cli10070097.

[12] R. Kumaraperumal, S. Pazhanivelan, K. P. Ragunath, B. Kannan, P. J. Prajesh, and G. R. Mugilan, "Agricultural drought monitoring in Tamil Nadu, India using satellite-based multivegetation indices," *J. Appl. Nat. Sci.*, vol. 13, no. 2, pp. 414–423, Jun. 2021, doi: 10.31018/jans.v13i2.2585.

[13] A. Srivastava, S. Umrao, and S. Biswas, "Exploring forest transformation by analyzing spatiotemporal attributes of vegetation using vegetation indices," *Int. J. Adv. Comput. Sci. Appl.*, vol. 12, no. 6, pp. 1–10, Jun. 2021.

[14] F. Shi, X. Gao, R. Li, and H. Zhang, "Ensemble learning for land cover classification of Loess Hills in the eastern Qinghai–Tibet Plateau using GF-7 multitemporal imagery," *Remote Sens.*, vol. 16, no. 14, pp. 1–12, Jul. 2024, doi: 10.3390/rs16142556.

[15] A. A. Khan, O. Chaudhari, and R. Chandra, "A review of ensemble learning and data augmentation models for class-imbalanced problems: Combination, implementation, and evaluation," *Expert Syst. Appl.*, vol. 232, pp. 1–28, Jun. 2024, doi: 10.1016/j.eswa.2023.122778.

[16] R. Al, F. Pulungan, and R. Nooraeni, "Comparative accuracies using machine learning models for mapping of sugarcane plantation based on Sentinel-2A imagery in Kediri area, East Java," *Int. J. Remote Sens. Earth Sci.*, vol. 21, no. 1, pp. 1–14, Jan. 2024.

[17] D. Demirtürk, Ö. Mintemur, and A. Arslan, "Optimizing LightGBM and XGBoost algorithms for estimating compressive strength in high-performance concrete," *Arab. J. Sci. Eng.*, Jan. 2025, doi: 10.1007/s13369-025-10217-7.

[18] I. M. Alkhawaldeh, I. Albalkhi, and A. J. Naswhan, "Challenges and limitations of synthetic minority oversampling techniques in machine learning," *World J. Methodol.*, vol. 13, no. 5, pp. 373–378, Dec. 2023, doi: 10.5662/wjm.v13.i5.373.

[19] A. Raja and T. Gopikrishnan, "Drought prediction and validation for desert region using machine learning methods," *Global Weather Research Series*, Jun. 2023. [Online]. Available: https://globalweather.tamu.edu/

[20] E. E. Başakın, P. C. Stoy, M. C. Demirel, M. Ozdogan, and J. A. Otkin, "Combined drought index using high-resolution hydrological models and explainable artificial intelligence techniques in Türkiye," *Remote Sens.*, vol. 16, no. 20, pp. 1–12, Oct. 2024, doi: 10.3390/rs16203799.

[21] A. de la I. Martinez and S. M. Labib, "Demystifying normalized difference vegetation index (NDVI) for greenness exposure assessments and policy interventions in urban greening," *Environ. Res.*, vol. 226, pp. 1–20, Mar. 2023, doi: 10.1016/j.envres.2022.115155.

[22] F. Salas-Martínez, O. A. Valdés-Rodríguez, O. M. Palacios-Wassenaar, A. Márquez-Grajales, and L. D. Rodríguez-Hernández, "Methodological estimation to quantify drought intensity based on the NDDI index with Landsat 8 multispectral images in the central zone of the Gulf of Mexico," *Front. Earth Sci.*, vol. 11, May 2023, doi: 10.3389/feart.2023.1027483.

[23] M. T. Paniagua, J. Villalba, and M. Pasten, "Spatial-temporal distribution of drought in the western region of Paraguay (2005–2017)," *Int. Arch. Photogramm. Remote Sens. Spatial Inf. Sci.*, vol. XLII-3-W12, pp. 327–330, Nov. 2020, doi: 10.5194/isprs-archives-XLII-3-W12-2020-327-2020.

[24] A. Mizen , "The use of enhanced vegetation index for assessing access to different types of green space in epidemiological studies," *J. Expo. Sci. Environ. Epidemiol.*, vol. 34, no. 5, pp. 753–760, Sep. 2024, doi: 10.1038/s41370-024-00650-5.

[25] M. Khan and R. Chen, "Assessing the impact of land use and land cover change on environmental parameters in Khyber Pakhtunkhwa, Pakistan: A comprehensive study and future projections," *Remote Sens.*, vol. 17, no. 1, pp. 1–12, Jan. 2025, doi: 10.3390/rs17010170.

[26] E. Ramadhan, F. Hadi, and M. A. Yusuf, "Spatio-temporal analysis of the effect of rainfall on carbon monoxide air pollution in Bandung City in 2023: A satellite data-based approach," *Jurnal Reka Lingkungan*, vol. 12, no. 3, pp. 269–282, Sep. 2024, doi: 10.26760/rekalingkungan.v12i3.269-282.

[27] I. H. Houmma , "A new multivariate agricultural drought composite index based on random forest algorithm and remote sensing data developed for Sahelian agrosystems," *Geomatics, Nat. Hazards Risk*, vol. 14, no. 1, pp. 1–12, Jun. 2023, doi: 10.1080/19475705.2023.2223384.

[28] K. Yamanada, Y. Matsuda, and J. Kuroiwa, "Optimal features for power usage prediction based on LightGBM," *Nonlinear Theory Appl. IEICE*, vol. 16, no. 3, pp. 401–409, Jul. 2025, doi: 10.1587/nolta.16.401.

[29] E. Gul, E. Staiou, M. J. S. Safari, and B. Vaheddoost, "Enhancing meteorological drought modeling accuracy using hybrid boost regression models: A case study from the Aegean region, Türkiye," *Sustainability*, vol. 15, no. 15, pp. 1–12, Aug. 2023, doi: 10.3390/su151511568.

[30] M. Lu , "A stacking ensemble model of various machine learning models for daily runoff forecasting," *Water*, vol. 15, no. 7, pp. 1–12, Apr. 2023, doi: 10.3390/w15071265.

[31] D. Boldini, F. Grisoni, D. Kuhn, L. Friedrich, and S. A. Sieber, "Practical guidelines for the use of gradient boosting for molecular property prediction," *J. Cheminform.*, vol. 15, no. 1, pp. 1–12, Dec. 2023, doi: 10.1186/s13321-023-00743-7.

[32] S. Ali , "Spatial downscaling of GRACE data based on XGBoost model for improved understanding of hydrological droughts in the Indus Basin Irrigation System (IBIS)," *Remote Sens.*, vol. 15, no. 4, pp. 1–12, Feb. 2023, doi: 10.3390/rs15040873.